Published in Journal of Physics : Condensed Matter 16, 3271-3278, 2004
which should be used for any reference to this work

Spin–orbit splitting in the valence bands of $1T$-TaS_2 and $1T$-$TaSe_2$

F Clerc[1], M Bovet[1], H Berger[2], L Despont[1], C Koitzsch[1], O Gallus[1], L Patthey[3], M Shi[3], J Krempasky[3], M G Garnier[1] and P Aebi[1]

[1] Institut de Physique, Université de Neuchâtel, CH-2000 Neuchâtel, Switzerland
[2] Institut de Physique Appliqué, EPFL, CH-1015 Lausanne, Switzerland
[3] Swiss Light Source, Paul Scherrer Institut, CH-5232 Villigen, Switzerland

E-mail: florian.clerc@unine.ch

Abstract

We perform angle-resolved photoemission spectroscopy on $1T$-TaS_2 and $1T$-$TaSe_2$ using synchrotron radiation. We observe a characteristic splitting of the chalcogen p-derived valence bands along high symmetry directions. Density functional theory calculation and group theory strongly suggest that this splitting is due to spin–orbit interaction along one direction, and to symmetry along the other direction. We note that, according to the Kramers degeneracy, the spin–orbit interaction leaves every state doubly degenerate. Furthermore, this study allows us to identify a mixing between bands with Ta 5d and Se 4p character, possibly relevant for the different temperature behaviours of the two compounds.

1. Introduction

Spin–orbit (SO) interaction is well known to be responsible for the splitting of degenerate electron energy levels in atoms, molecules and solids. In the past it has played an important role in describing the band structure of semiconductors [1, 2], and more recently in explaining various splittings of surface states [3–7]. Its physical origin is relativistic, and can be explained by the interaction of the magnetic momentum of the electron (spin) with the magnetic field viewed by this electron because of its movement in the electrostatic field of the proton. This gives an additional term to the Schrödinger equation which takes the form $H_{\mathrm{SO}} = (\hbar/4mc^2)(\vec{\nabla}V \times \vec{p}) \cdot \vec{\sigma}$, where V is the external potential, $\vec{p}$ is the momentum, and $\vec{\sigma}$ is the Pauli spin operator. It can also be written in the more friendly form $H_{\mathrm{SO}} \sim L \cdot S$, where L and S are the orbital and spin angular momenta, respectively [8].

Here we report high resolution angle-resolved photoemission (ARPES) measurements performed on $1T$-TaS_2 and $1T$-$TaSe_2$ at room temperature. ARPES is a powerful tool for studying the energy and momentum distribution of electrons. The technical progress made

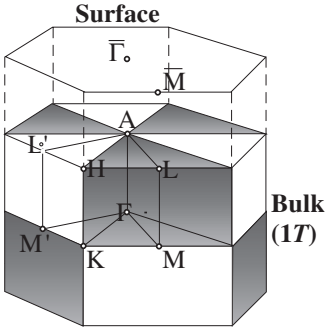

Figure 1. Surface and bulk Brillouin zones of the $1T$ structure.

constantly to improve the resolution of the measurements continues to refine the information, allowing a better understanding of the physics behind materials. $1T$-TaS_2 and $1T$-$TaSe_2$ have attracted much attention because of their quasi-two dimensionality and the presence of charge density waves (CDW) [9]. The comparison between these two compounds has also been largely investigated because, despite their similar crystal structure and CDW symmetry, they exhibit different physical properties [10–12]. Indeed, $1T$-TaS_2 shows two successive first order transitions, from incommensurate CDW (ICCDW) to nearly commensurate CDW (NCCDW) at about 350 K, and from NCCDW to commensurate CDW (CCDW) at about 180 K. In particular, it appears that this latter transition is closely related to a Mott localization within the Ta 5d band [13]. On the other hand, $1T$-$TaSe_2$ undergoes an ICCDW to CCDW transition at about 430 K, but does not exhibit a bulk metal–insulator transition at low temperature. In this paper we focus our discussion on the chalcogen (S, Se) p-derived valence bands where a characteristic double peak is visible in the ARPES spectra. To explain this splitting we compare self-consistent full potential linearized augmented plane wave (FLAPW) calculations performed with and without considering spin–orbit coupling (SOC). The calculations strongly suggest that SOC is at the origin of the splitting, but only in the centre of the Brillouin zone (BZ) (Γ), and along Γ–A (see figure 1). We complete our investigation with group theory. Group theory provides methods for obtaining qualitative information about degeneracies of electron energy levels and crystal wavefunctions only from symmetry considerations [14, 15]. This study confirms and allows a better understanding of the results from FLAPW calculations.

2. Experiment and calculation

Photoemission measurements were carried out at room temperature using a high resolution angle-resolved photoemission spectrometer (SES-2002) at the SIS beamline X09LA of the Swiss Light Source. The energy and angular resolutions were below 10 meV and $\pm 0.3°$, respectively. Pure $1T$-TaS_2 and $1T$-$TaSe_2$ samples were prepared by vapour transport [16, 17] and cleaved *in situ* at pressures in the lower 10^{-10} mbar region. The quality and the orientation of the crystal structure were checked by low energy electron diffraction (LEED). The electronic structure calculations are made using the WIEN package [18], implementing the FLAPW method within the framework of density functional theory (DFT). The generalized gradient approximation was used for the exchange–correlation potential [19]. SOC has been included in the calculations in a second variational step as explained in [20]. For both samples the calculations are performed for the non-reconstructed (without CDW) crystallographic structure with space group $P\bar{3}m1$. The lattice parameters are $a = b = 3,36$ Å, $c = 5,85$ Å and $a = b = 3,48$ Å, $c = 6,27$ Å for the $1T$-TaS_2 and $1T$-$TaSe_2$, respectively.

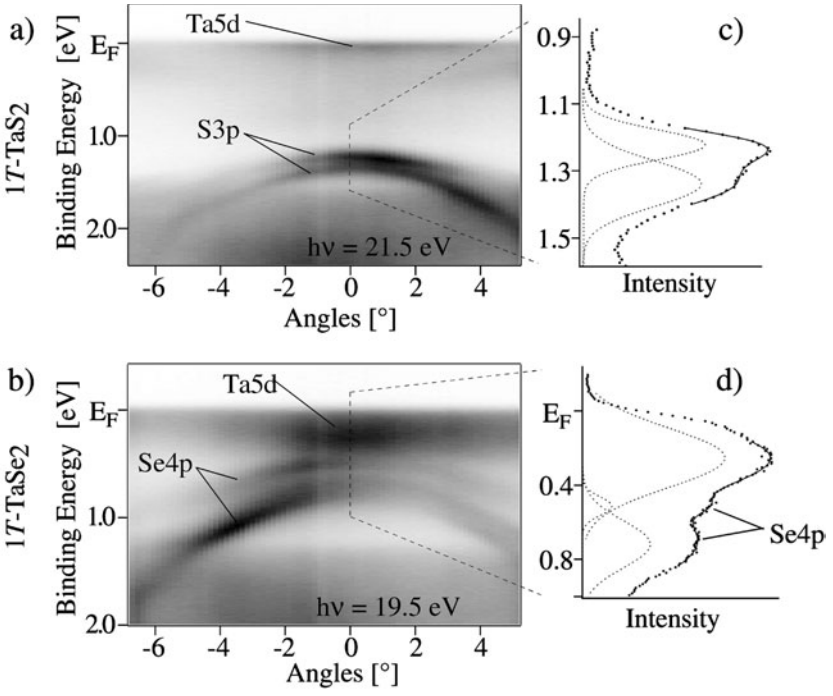

Figure 2. Carpets for $1T$-TaS_2 (a) and $1T$-$TaSe_2$ (b). (c) and (d) EDCs extracted at Γ from the carpet. The black lines correspond to the fit function resulting from the sum of the Gaussians in dotted grey lines.

3. Results and discussion

Figures 2(a) and (b) show carpets, (sets of energy distribution curves (EDCs) plotted in grey scale with high intensity in black) measured within the Γ ALM plane along the high symmetry direction $\bar{\Gamma}$–$\bar{\mathrm{M}}$ of the hexagonal surface BZ, for $1T$-TaS_2 and $1T$-$TaSe_2$ with photon energies of 21.5 and 19.5 eV, respectively. In $1T$-TaS_2 the chalcogen p-derived bands are largely separated from the Ta 5d-derived bands which lie near the Fermi level, in contrast to what we see for $1T$-$TaSe_2$, where the Se p-derived bands and the Ta 5d-derived bands are very close. It is clear from these data that both S 3p-derived bands and Se 4p-derived bands are split. This splitting is minimal at normal emission (0°) but still visible, as can be seen on the fits of the normal emission spectra shown in figures 2(c) and (d) (vertical cuts across the carpet). To explore the evolution of these bands along the Γ–A direction the measurements are repeated for different photon energies. The results are presented in figures 3(a) and (b), where we show the peak positions obtained from the fit functions of the vertical cuts at normal emission (e.g., the white circles on the curves (figures 3(a), (b)) correspond to the peak positions found in figures 2(c) and (d)). A free electron photoemission final state, as plotted in figures 3(c) and (d), is assumed to determine the k-point within the BZ[4]. For the split S 3p-derived bands (figure 3(a)) we obtain two parallel bands over the whole measured region and a constant splitting of the order of 100 meV. For the Se 4p-derived bands (figure 3(b)), the upper band position passes

[4] The k-point positions are calculated using the usual photoemission formula $k = \sqrt{0.263(\hbar\omega - E_\mathrm{B} - \phi + V_0)}$ with $\hbar\omega$, E_B, ϕ and V_0 denoting the photon energy, the binding energy, the sample work function and the inner potential, respectively. We assume the following reasonable values $V_0 = 13$ eV, $\phi = 3.5$ eV and $E_\mathrm{B} = 1.3$ eV for $1T$-TaS_2 and $V_0 = 11$ eV, $\phi = 3.5$ eV and $E_\mathrm{B} = 0.5$ eV for $1T$-$TaSe_2$.

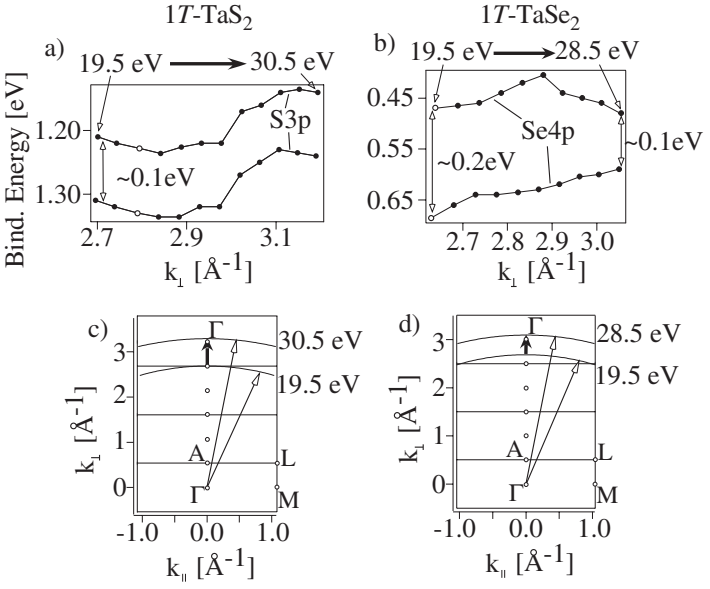

Figure 3. Dispersion of the split chalcogen p-derived bands along the Γ–A direction for $1T$-TaS_2 (a) and $1T$-$TaSe_2$ (b). The white circles correspond to the peak positions found from the fit in figures 2(c) and (d). The other peak positions are determined in the same manner but from EDCs taken at different photon energies. A cut in reciprocal space for $1T$-TaS_2 (c) and $1T$-$TaSe_2$ (d) with free electron final state wavevectors for various photon energies. The black arrows show the region measured by changing the photon energy.

through a maximum, whereas the lower band position increases constantly. This results in a change of the magnitude of the splitting from 200 meV near A to 100 meV near Γ.

Band structure calculations performed without considering the SOC are presented in figures 4(a) and (b). In grey are represented the Ta 5d-derived bands near the Fermi level in the Γ–A region and in black at 1 eV, and 0.2 eV binding energy, respectively, the S and Se p-derived bands.

The most interesting observation is that the calculated S and Se p-derived bands are split along Γ–M but not along Γ–A, indicating that the measured splittings of the chalcogen p-bands have different physical origin, and we can already say that the splitting along Γ–M is due to the crystal field and has its origin in the symmetry. However, the splitting along Γ–A observed in our measurements is reproduced by the calculations of figures 4(c) and (d) where the SOC was accounted for. Indeed, for the two materials, as we can see in the region delimited by the grey rectangles, the calculations reproduce the behaviour of the bands measured in figures 3(a) and (b) well. The magnitude of 100 and 360 meV for the splitting predicted by the calculations is in good agreement for $1T$-TaS_2 but exaggerated in the case of $1T$-$TaSe_2$. For $1T$-$TaSe_2$ an additional effect of the introduction of SOC in the calculation is the crossing between the upper Se 4p-derived band and the lower Ta 5d-derived band. Therefore, the upper measured band in figure 3(b) is the upper Se 4p-derived band from $k_\perp = 2.64$ to 2.88 Å^{-1} (the crossing point) and the lower Ta 5d-derived band from $k_\perp = 2.88$ to 3.05 Å^{-1}. Thus we measure a splitting only up to this crossing point, then the upper Se band is no longer visible. This mixing or hybridization (confirmed here by the measurement) between Ta and Se derived bands has played an important role in explaining the differences in physical properties of the isostructural $1T$-TaS_2 and $1T$-$TaSe_2$ [11].

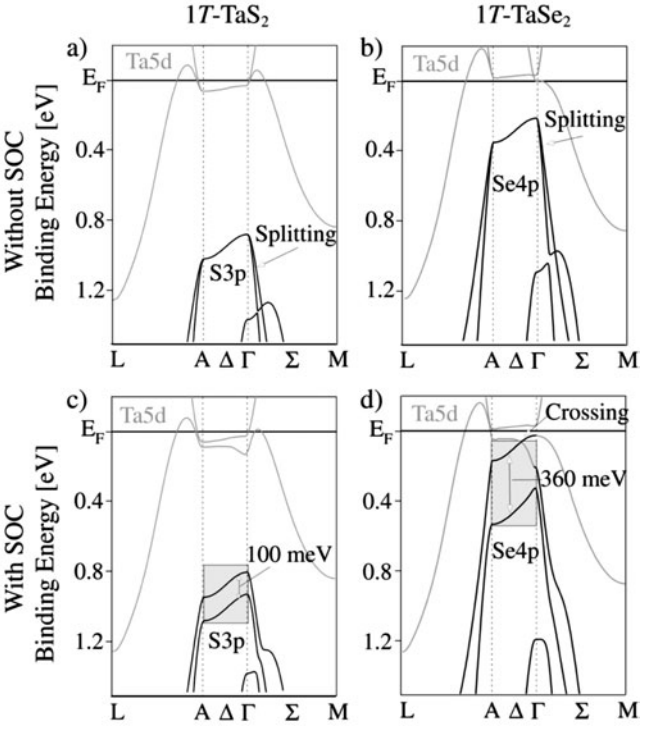

Figure 4. (a)–(d) Calculated band structures. In the calculations with SOC (c) and (d) the regions corresponding to figures 3(a) and (b) are shaded in grey.

For quantitative information, as shown for the study of SOC in semiconductors [1], the atomic splitting is a good indicator for the magnitude of the SO splitting in valence bands. The atomic splitting of the 3p level in S is 95 meV [21]. This value is of the same order as the magnitude measured for the S 3p-derived valence band, which confirms the isolated character of the S atoms in $1T$-TaS_2. The splitting of the 4p level in Se is 418 meV [21], approximately twice as large as the measured SO splitting. This reduction of the splitting in the Se 4p valence band may be a consequence of the mixing with the Ta 5d bands, where the electrons not only feel the Se nuclei but are also influenced by the Ta nuclei. A similar anomaly in SO splitting has already been seen in semiconductors [22].

Therefore, the comparison between band structure calculation and ARPES measurements immediately suggests that the splitting along Γ–M is the result of symmetry, whereas the SO interaction causes the splitting along Γ–A. The major difference between the two compounds lies in the interaction of the chalcogen atoms with the Ta. Whereas we can neglect this interaction for $1T$-TaS_2, there is a strong mixing between Ta 5d-derived bands and Se 4p-derived bands. This can explain in part the relatively weak splitting found in $TaSe_2$. The discrepancy between calculation and measurements for the magnitude of the Se 4p-derived band splitting can be explained by the introduction of SOC as a perturbative calculation in the Wien code.

Now we will show that the same conclusions about the origin of these splittings can be obtained with only a few considerations using group theory. Group theory gives us tools to deduce some of the properties of the energy levels of electrons in the crystal without solving the corresponding Schrödinger equation. To understand how the symmetry properties of a

solid help us to extract some information about the solutions of the Schrödinger equation $H\psi = E\psi$, we just give a short reminder below. Consider a set of degenerate solutions ψ_i^μ of the Schrödinger equation. We have $H\psi_i^\mu = E_\mu\psi_i^\mu$, for $i = 1, \ldots, n_\mu$. This set of eigenfunctions forms a function space associated with the eigenvalue E_μ. Now the key point, as H is invariant under all the transformation operators $\Re$ corresponding to the symmetry operations R of the considered symmetry group ($[H, \Re] = 0$), $\Re\psi_j^\mu$ is also an eigenfunction of H with eigenvalue E_μ. It follows that $\Re\psi_j^\mu$ is a member of the function space for energy E_μ. We can then write $\Re\psi_j^\mu = \sum_{i=1}^{n_\mu} D_{ij}^\mu(R)\psi_i^\mu$, $j = 1, \ldots, n_\mu$. In this manner a set of matrices $D^\mu(R)$ is built which is homomorphic with the symmetry group. This set of matrices forms a representation of the symmetry group, and the linearly independent degenerate wavefunctions ψ_i^μ for energy level E_μ form a basis for the representation called Γ^μ. Since we know all the irreducible representations of the symmetry group we can deduce some information about the possible solutions of the Schrödinger equation. As a matter of fact each energy level corresponds to an irreducible representation, and the dimension of this representation gives the degree of degeneracy of this level. How do we build these irreducible representations without knowing the solutions ψ_i? Group theory, with the use of mathematical rules, allows us to construct character tables of the symmetry group and to extract from these tables the properties of the irreducible representations. In the case of a crystal, all the symmetry information is contained in the space group which is, according to the international notation, $P\bar{3}m1$ for $1T$-TaS_2 and $1T$-$TaSe_2$. The tables for single and double groups (the ones necessary for SOC) of this space group are not displayed here but are available in [23]. To denote the representations of the group of vector $\vec{k}$ we follow the notation of [23]. We assume that the p chalcogen valence bands are derived only from the three S and Se p_x, p_y, p_z orbitals. This is an approximation but we might expect that for $\vec{k}$ vectors of high symmetry these orbitals give a reasonable description of the wavefunctions. First, we begin by neglecting the spin of the electron (study without SOC) and we restrict the study of the degeneracy to the three $\vec{k}$ vectors Γ (centre of BZ), Δ (any intermediate point on the line Γ–A) and Σ (point along Γ–M). The results obtained from this study (without SOC) in the framework of the group theory are summarized in figure 5(a) and, for the case with SOC, in figure 5(b). The irreducible character table of the group of Γ [23] shows directly that the orbital p_z belongs to the irreducible representation $\Gamma_2^-(1)$, where the number in parentheses (i.e. (1)) indicates the dimension of the representation, and that the orbitals p_x and p_y form a basis of the irreducible representation $\Gamma_3^-(2)$. Hence, there are two 'bands' in Γ, one non-degenerate and one doubly degenerate. The use of the compatibility rule shows that the degeneracy stays the same along Δ but that the doubly degenerate Γ_3^- level is split along Σ in two non-degenerate states. This corresponds exactly to the behaviour observed in the calculations (figures 4(a) and (b)), and confirms that the splitting along Γ–M is a consequence of the lowering of symmetry from Γ to Σ.

Now we observe the effect of introducing SOC. First we note that adding spin simply doubles the degeneracy of every state. But when SOC is turned on more dramatic changes in the bands can occur, such as the lifting of degeneracies. If this is the case, inspection of the character table has to predict these effects. In terms of group theory, the introduction of SOC implies that we have to work with the double groups introduced by Bethe [24]. In other words the eigenfunctions of the Hamiltonian containing the SOC term ($H + H_{SOC}$) form a basis for the irreducible representations of the double group. To find these irreducible representations we proceed as follows. We start from the irreducible representations (Γ_{SG}) of the single group found in the previous study without SOC (i.e. for the k-point Γ: $\Gamma_2^-(1)$ and $\Gamma_3^-(2)$). To each of these representations (Γ_{SG}) corresponds an irreducible representation (Γ_{DG}) of the double group which can be identified straightforwardly by comparing the characters. For the k-point

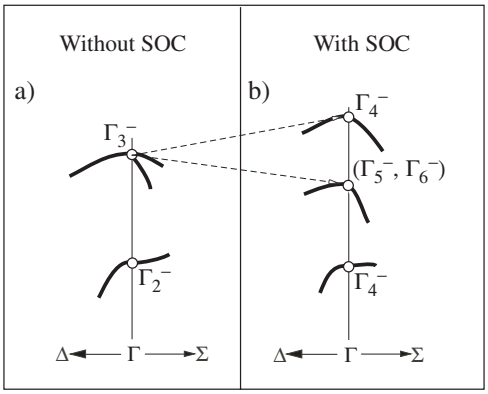

Figure 5. The schematic band structure obtained from group theory (see text).

Γ, the representation $\Gamma_{SG} = \Gamma_2^-$ induces the representation of the double group $\Gamma_{DG} = \Gamma_2^-$, and $\Gamma_{SG} = \Gamma_3^-$ induces $\Gamma_{DG} = \Gamma_3^-$. As we introduce the spin, the eigenfunctions are no longer linear combinations of only the p_x, p_y, p_z orbitals, but the product of these orbitals with the spin functions α and β. Thus we have to identify for which irreducible representation Γ_S (S for spin) of the considered double group the spin functions α and β form a basis. For the double group of the k-point Γ, $\Gamma_S = \Gamma_4^+$. Finally the irreducible representations of the double group for which the eigenfunctions of the Hamiltonian $H + H_{SOC}$ form a basis result from the reduction (if necessary) of the representation obtained by the direct product $\Gamma_{DG} \otimes \Gamma_S$. For the k-point Γ we get the following: $\Gamma_2^- \otimes \Gamma_4^+ = \Gamma_4^-(2)$ and $\Gamma_3^- \otimes \Gamma_4^+ = \Gamma_5^-(1) + \Gamma_6^-(1) + \Gamma_4^-(2)$.

These results show that the introduction of SOC doubles the degeneracy of the band Γ_2^- and splits the band Γ_3^- into two non-degenerate and one doubly degenerate bands. However, this last result seems to be in contradiction with the Kramer degeneracy (each level of a system containing time reversal symmetry and inversion symmetry is at least doubly degenerate [8]). But in fact the two representations Γ_5^- and Γ_6^- correspond to the same energy. Hence Γ_3^- splits into two doubly degenerate bands. We again use the compatibility rule to show how the degeneracy evolves when moving from Γ to Σ or Δ. Along Σ, SOC simply doubles the degeneracy of the three distinct bands, and along Δ, the behaviour is similar to that at Γ. To summarize, the most important effect of SOC is the splitting at Γ and Δ of the level Γ_3^- into two bands (Γ_5^-, Γ_6^-) and Γ_4^-. The origin of this SO splitting is even more clearly illustrated by calculating, using the projection method, the basis functions of these representations obtained from the six p orbitals (taking into account spin) and changing the basis in the more adapted JM_J basis (total angular momentum, projection of this angular momentum). This shows that the basis functions of $\Gamma_5^- + \Gamma_6^-$ are pure $J = 3/2$ states, whereas the basis functions of Γ_4^- are a mixing of $J = 1/2$ and $3/2$ states.

4. Conclusion

Our ARPES measurements exhibit a splitting of the chalcogen p-derived valence bands along the high symmetry directions A–Γ–M in $1T$-TaS_2 and $1T$-$TaSe_2$. Based on density functional theory calculations, we attribute this splitting to the symmetry along Γ–M and to the SO interaction along Γ–A. The introduction of SOC has a considerable effect on the band structure; in particular, it splits the degenerate bands along the $k_\perp$ direction (Γ–A) of the S–Se p-derived bands, the splitting along Γ–M being already reproduced by a non-relativistic calculation. For

completeness and understanding we have studied the effect of the SO within the framework of group theory. This has the advantage of describing the evolution of the degeneracies of the chalcogen bands which, for simplicity, are constructed purely from p orbitals. We note that although the SO interaction lifts one degeneracy, it still leaves all states doubly degenerated due to the presence of inversion symmetry. It is a well known fact that the SO interaction does not separate states of opposite spin if the lattice potential has a centre of inversion [8]. This is not the case at the crystal surface and, for example, it has been observed that SOC is responsible for a spin splitting of surface state bands leading to non-degenerate states [3, 7]. Finally, this study allows us to identify a key difference between $1T$-TaS_2 and $1T$-$TaSe_2$, namely the strong mixing between the Ta 5d and Se 4p derived bands.

Acknowledgments

Skillful technical assistance was provided by O Raetzo, E Mooser, R Schmid, O Zosso, Ch Neururer, and F Bourqui. This project has been supported by the Fonds National Suisse de la Recherche Scientifique.

References

[1] Kane E O 1956 *J. Phys. Chem. Solids* **1** 82
[2] Braunstein R and Kane E O 1962 *J. Phys. Chem. Solids* **23** 1423
[3] LaShell S, McDougall B A and Jensen E 1996 *Phys. Rev. Lett.* **77** 3419
[4] Petersen L and Hedegard P 2000 *Surf. Sci.* **459** 49
[5] Nicolay G *et al* 2002 *Phys. Rev.* B **65** 033407
[6] Henk J, Ernst A and Bruno P 2003 *Phys. Rev.* B **68** 165416
[7] Rotenberg E, Chung J W and Kevan S D 1999 *Phys. Rev. Lett.* **82** 4066
[8] Ziman J M 1979 *Principles of the Theory of Solids* (Cambridge: Cambridge University Press)
[9] Wilson J A, Di Salvo F J and Mahajan J 1975 *Adv. Phys.* **24** 117
[10] Smith N V and Traum M M 1975 *Phys. Rev.* B **11** 2087
[11] Horiba K *et al* 2002 *Phys. Rev.* B **66** 073106
[12] Bovet M *et al* 2004 *Phys. Rev.* B **69** 125117
[13] Fazekas P and Tossati E 1979 *Phil. Mag.* B **39** 229
[14] Bouckaert L P, Smoluchowski R and Wigner E 1936 *Phys. Rev.* **50** 58
[15] Altmann S L 1994 *Band Theory of Solids: an Introduction From Point of View of Symmetry* (Oxford: Oxford University Press)
[16] Dardel B *et al* 1992 *Phys. Rev.* B **45** 1462
[17] Dardel B *et al* 1992 *Phys. Rev.* B **46** 7407
[18] Blaha P, Schwarz K and Luitz J 1999 *WIEN97 A Full Potential Linearized Augmented Plan Wave Package for Calculating Crystal Properties* Karlheinz Schwarz, Techn. University Wien, Austria (ISBN 3-9501031-0-4) This is an improved and updated Unix version of the original copyrighted WIEN code, which was published by Blaha P, Schwarz K, Sorantin P and Trickey S B 1990 *Comput. Phys. Commun.* **59** 399
[19] Perdew J P, Burke S and Ernzerhof M 1996 *Phys. Rev. Lett.* **77** 3865
[20] Singh D 1994 *Plane Waves, Pseudopotentials and the LAPW Method* (Dordrecht: Kluwer–Academic)
[21] Herman F and Skillman S 1963 *Atomic Structure Calculations* (Englewood Cliffs, NJ: Prentice-Hall)
[22] Cardona M and Christensen N E 2000 *Solid State Commun.* **116** 421
[23] Bradley C J and Cracknell A P 1972 *The Mathematical Theory of Symmetry in Solids* (Oxford: Clarendon)
[24] Bethe H A 1929 *Ann. Phys., Lpz.* **3** 133–208